Coupled channel analysis of neutron transfer in ^{6,7}Li induced reactions around the Coulomb barrier*

Himanshu Sharma Rishabh Kumar Moumita Maiti†

Department of Physics, Indian Institute of Technology Roorkee, Roorkee- 247667, Uttarakhand, India

Abstract: The coupled reaction channel approach has proven to be quite effective in explaining the mechanism of nucleon transfer in heavy-ion reactions. Nevertheless, significant ambiguities remain regarding the selection of potential parameters and the states of the nuclei that should be coupled together for a specific reaction channel. In this study, the excitation functions for one- and two-neutron transfer in ^{6,7}Li-induced reactions on various targets were analyzed using the coupled reaction channel formalism. Spectroscopic amplitudes were taken from the existing literature and shell model calculations. The one-neutron transfer cross sections from ^{6}Li+^{93}Nb and ^{7}Li+^{115}In reactions were reasonably well reproduced by coupled reaction channel calculations. A reasonable match for the measured cross sections was also obtained for the two-neutron transfer in the ^{7}Li+^{181}Ta reaction by employing the extreme cluster model.

Keywords: transfer reaction, cross section, weakly bound nuclei

DOI: 10.1088/1674-1137/ad99ae **CSTR:** 32044.14.ChinesePhysicsC.49034109

I. INTRODUCTION

The atomic nucleus is a complex many-body system. Understanding the internal degrees of freedom is essential for comprehending nuclear structure characteristics such as single-particle and collective states, clustering, and pairing correlations [1]. The information about the internal degrees of freedom is obtained from direct nuclear reactions, such as elastic scattering, inelastic scattering, and nucleon transfer, which are necessary to understand the stability of nuclei. Transfer reactions are also effective for producing neutron-rich nuclei [2, 3]. Further, the availability of radioactive beams has enabled the investigation of direct nuclear reactions in regions far from stability [4, 5].

Over the past decades, transfer reactions have been extensively studied. Single nucleon transfer provides insights into the shell structure, whereas two nucleon transfer reactions are particularly useful for exploring pairing correlations [6, 7]. The optical potential (OP) and spectroscopic factors are essential parameters for calculating transfer cross sections. Stripping reactions such as(d,p) [8, 9] and (t,d) [10] are extensively used in nuclear structure studies to investigate the spectroscopic factor. ^{6}Li and ^{7}Li are commonly recognized as weakly bound nuclei having cluster structures, such as $d+\alpha$ and $t+\alpha$. Thus, similar reaction mechanisms can be expected for (^{6}Li, ^{5}Li) and (d,p) reactions, as well as (^{7}Li, ^{6}Li) and (t,d) reactions, assuming that the α particle does not participate in the neutron transfer process. Consequently, the same structural information can be obtained using (^{6}Li, ^{5}Li) and (^{7}Li, ^{6}Li) reactions. Spectroscopic factors were traditionally determined by comparing calculated and measured transfer reaction cross sections. However, this experimental approach can introduce ambiguities due to the chosen OPs and coupling scheme used in the calculations. With the remarkable increase in computing power, detailed nuclear structure calculations, such as large-scale shell-model computations, are currently being used to determine spectroscopic factors. Moreover, significant progress has been made in reaction theory. The distortion of the incoming and outgoing scattering waves is now effectively managed by using double-folding OPs, such as the São Paulo potential (SPP), in the transfer reactions [11, 12].

Because direct transfer and breakup do not require tunneling through the barrier, their excitation functions do not decrease as rapidly as the fusion excitation function at sub-barrier energies. Consequently, the cross sections for these processes may be larger than the fusion cross sections. In the ^{6,7}Li+^{198}Pt systems, measurements have shown that the direct reaction cross section is signi-

Received 8 November 2024; Accepted 2 December 2024; Published online 3 December 2024

* Himanshu Sharma acknowledges the MHRD Research Fellowship, and Rishabh Kumar acknowledges the DST INSPIRE (IF180078) Research Fellowship from the Government of India

† E-mail: moumita.maiti@ph.iitr.ac.in

ficantly larger than the fusion cross section at sub-barrier energies for ^{6}Li+^{198}Pt [13]. For ^{7}Li+^{198}Pt, scholars found that both one- and two-neutron stripping and one-neutron pickup reactions play significant roles [14]. Similarly, large transfer cross sections have been observed in ^{6,7}Li+^{197}Au and ^{6}Li+^{181}Ta reactions [15, 16]. The derived excitation function drops less steeply compared to the complete fusion excitation function at low energy in one-neutron stripping reactions of ^{6}Li+^{96}Zr. Experimental findings involving neutron-halo nuclei such as ^{6,8}He [17−19] indicate that one- and two-neutron transfer channels are the predominant non-elastic processes below the Coulomb barrier and remain significant at energies above the barrier.

However, the mechanism behind the transfer of nucleons between a projectile and a target still has multiple aspects to be understood. It becomes more complicated due to processes such as sequential transfers and inelastic excitations that can occur before or after the transfer, alongside the typically dominant direct cluster transfer. With more nucleons involved, possible interactions escalate, further complicating the understanding of the reaction mechanism. In the literature, authors have commonly noted in ^{6,7}Li-induced reactions that the measured excess cross sections in pxn- or αxn-channels compared to the theoretical predictions are primarily attributed to incomplete fusion, with direct transfer often being overlooked [20−24]. Besides the breakup process, which is associated with the low binding energies of α particles, the significance of neutron transfer has been highlighted due to its substantial contribution to the production of inclusive α cross sections [25, 26]. Although numerous studies have concentrated on the breakup process, the role of neutron transfer still needs to be explored. Measurements of neutron transfer cross sections using weakly bound projectiles are limited, and available data are sparse [26−32].

In this study, we investigated one-neutron transfer in the ^{6}Li+^{93}Nb and ^{7}Li+^{115}In systems, as well as two-neutron transfer in the ^{7}Li+^{181}Ta system, utilizing the coupled reaction channel (CRC) formalism. We analyzed the impact of coupling between various reaction channels and studied the relative contributions from the transfer path to understand the reaction mechanism. The remainder of this article is organized as follows. The explanations of the formalism, shell model, and CRC calculations are outlined in Sect. II. Section II D presents a discussion, and our work is summarized and concluded in Sect. III.

II. THEORETICAL ANALYSIS AND DISCUSSION

A. Brief description of the formalism

The theoretical formalism for one-neutron transfer is discussed in this section. The formalism for two-neutron transfer is similar to that for one-neutron transfer, with a distinction that the pair of neutrons behave like a single quasi-particle and the transition potential is assumed to act on the relative motion between the correlated neutron pair and the core.

For one-neutron transfer in the reaction ($a+A\rightarrow b+B$), the wave functions of the entrance and exit channels can be represented as $\Psi_{\alpha}(R,\zeta_i,\zeta_j)$ and $\Psi_{\beta}(R',\zeta_k,\zeta_l)$. Here, R and R' denote the center of mass coordinates between the projectile and the target in the entrance and exit channels. The intrinsic coordinates of a and b are denoted as ζ_i and ζ_k, respectively, whereas those of A and B are represented by ζ_j and ζ_l, respectively. Consequently, the transfer matrix elements, which are used to calculate the coupling terms that arise from the transfer of particles, can be expressed as follows:

$$T_{\alpha\beta}=\left\langle\Psi_{\beta}\right|W_{\alpha}\left|\Psi_{\alpha}\right\rangle. \tag{1}$$

Here, $|\Psi_{\alpha}\rangle=\sum_{ij}\left|\phi_{a_i}\phi_{A_j}\chi_{\alpha}\right\rangle$ and $\left\langle\Psi_{\beta}\right|=\sum_{kl}\left\langle\phi_{b_k}\phi_{B_l}\chi_{\beta}\right|$. The symbol ϕ represents the intrinsic wave functions of the nuclei, whereas χ_{α} and χ_{β} denote the relative motion wave functions in entrance and exit channels. a_i, A_j, b_k, and B_l are all the quantum numbers required to specify the state of the a, A, b, and B nuclei.

The residual interaction, in the prior form, is given by $W_{\alpha}=U_c(R_c)+v(r')-U(R)$. Here, $U_c(R_c)$, where R_c denotes the distance between centers of nuclei, represents the core-core potential. The OP $U(R)$ is used to generate the corresponding distorted waves. Both $U_c(R_c)$ and $U(R)$ are complex potentials defined to describe the scattering between core nuclei and between the projectile and target in the entrance channel. The term $U_c(R_c)-U(R)$ is called the residual remnant potential. $v(r')$ is the real potential that binds the valence nucleon to the core.

In this work, we used the SPP as the OP, which is derived from a double-folding form:

$$V_F(R)=\int\rho_1(r_1)v_{NN}(R-r_1+r_2)\rho_2(r_2)\mathrm{d}r_1\mathrm{d}r_2. \tag{2}$$

In Eq. (2), r_i (i=1,2) represents the vector that connects the center of mass of nucleus i to the respective volume element, whereas R connects the centers of masses of the two nuclei. ρ_1 and ρ_2 are the matter densities of the colliding nuclei, and $v_{NN}(R-r_1+r_2)$ is the nucleon-nucleon M3Y interaction [33, 34]. The SPP is given by $V^{SP}(R,E)=V_F(R)\mathrm{e}^{-4v^2/c^2}$ [35], where v is the relative velocity between the colliding nuclei, and c is the speed of light.

The intrinsic wave functions for a nucleus B consisting of a core A and a valence particle v are expressed as follows:

$$\phi_B^{JM}(\zeta_l, r) = \sum_{Ilj} A_{lsj}^{IJ}[\phi_A^I(\zeta_j) \otimes \phi_{lsj}(r)]_{JM}, \quad (3)$$

where $\phi_{lsj}(r)$ is the bound wave function of the valence particle with quantum numbers (l, s, j). The spectroscopic amplitudes A_{lsj}^{IJ} are connected to the spectroscopic factors S_{lsj}^{IJ}, where $S_{lsj}^{IJ} = |A_{lsj}^{IJ}|^2$. The spectroscopic factors represent the probability of finding the valence particle v in a single-particle state defined by (l, s, j), coupled to a core A with spin I. The core wave function is denoted as $\phi_A^I(\zeta_j)$. To calculate transfer amplitudes, CRC codes typically require the spectroscopic factors and quantum numbers (l, s, j) of the valence particle to construct the wave functions of the composite particle, along with the coupling potentials for valence-core and core-target interactions.

B. Shell model calculations

The spectroscopic amplitudes for the projectile and target overlaps are essential for performing microscopic CRC calculations. These amplitudes were obtained through shell-model calculations using the NuShellX code [36]. For the system ^{6}Li+^{93}Nb, to acquire the one-neutron spectroscopic information for the target overlaps, the calculations were performed with the *sn* model space and the effective interaction *snet*. In this model space, the ^{56}Ni nucleus is considered a closed core, and the $1f_{5/2}$, $2p_{3/2}$, $2p_{1/2}$, $1g_{9/2}$, $1g_{7/2}$, $2d_{5/2}$, $2d_{3/2}$, and $3s_{1/2}$ orbitals are treated as the valence space for neutrons and protons. However, constraints were necessary due to our computational limitations in performing the shell-model calculations with such a large valence space. Consequently, we imposed some restrictions and considered the nucleus ^{88}Sr as a closed core instead of ^{56}Ni. This truncation made the accessible valence orbitals for neutrons $1g_{7/2}$, $2d_{5/2}$, $2d_{3/2}$, and $3s_{1/2}$, and for protons, the accessible valence orbitals became $2p_{1/2}$, $1g_{9/2}$, $1g_{7/2}$, $2d_{5/2}$, $2d_{3/2}$, and $3s_{1/2}$. For the projectile overlaps, both the $1p_{3/2}$ and $1p_{1/2}$ components of the neutron bound to ^{6}Li were included, with spectroscopic factors of 0.43 and 0.29 [37]. Table 1 presents the spectroscopic amplitudes used in the one-neutron transfer calculations related to the target overlaps. Table 2 compares the excitation energies derived from the *snet* interactions and the experimental values.

Table 1. Spectroscopic amplitudes used in one-neutron transfer CRC calculations for ^{6}Li+^{93}Nb reaction, where j is the spin of the neutron orbitals.

Initial State	j	Final State	Spect. Ampl.
^{93}Nb$_{g.s.}(9/2^+)$	$2d_{5/2}$	^{92}Nb$_{g.s.}(7^+)$	0.7265
	$1g_{7/2}$		0.0520
^{93}Nb$_{g.s.}(9/2^+)$	$2d_{5/2}$	^{92}Nb$_{0.136}(2^+)$	0.5372
	$1g_{7/2}$		0.06
^{93}Nb$_{g.s.}(9/2^+)$	$2d_{3/2}$	^{92}Nb$_{0.286}(3^+)$	0.0557
	$2d_{5/2}$		0.3951
	$1g_{7/2}$		0.01
^{93}Nb$_{g.s.}(9/2^+)$	$3s_{1/2}$	^{92}Nb$_{0.357}(5^+)$	0.1575
	$2d_{3/2}$		0.0374
	$2d_{5/2}$		0.4287
	$1g_{7/2}$		0.0245
^{93}Nb$_{g.s.}(9/2^+)$	$3s_{1/2}$	^{92}Nb$_{0.480}(4^+)$	0.1034
	$2d_{3/2}$		0.0361
	$2d_{5/2}$		0.3763
	$1g_{7/2}$		0.0346
^{93}Nb$_{g.s.}(9/2^+)$	$2d_{3/2}$	^{92}Nb$_{0.501}(6^+)$	0.0412
	$2d_{5/2}$		0.3681
	$1g_{7/2}$		0.0264

Table 2. Comparison of experimental and NuShellX results for ^{92}Nb and ^{93}Nb spectra using the *snet* interactions. The spin and parity of states are denoted as j^π.

Nucleus	j^π	Energy/MeV	
		Experimental	*snet* interaction
^{92}Nb	7^+	0.0	0.0
	2^+	0.136	0.168
	3^+	0.286	0.316
	5^+	0.357	0.288
	4^+	0.480	0.431
	6^+	0.501	0.459
^{93}Nb	$9/2^+$	0.0	0.0
	$1/2^-$	0.031	0.171
	$5/2^+$	0.809	1.053
	$5/2^-$	0.810	1.066

C. CRC calculations

1. *One-neutron transfer*

In this study, we analyzed the experimental excitation functions of the residues ^{92m}Nb, populated in ^{6}Li+^{93}Nb reactions [21], as well as ^{116m}In in ^{7}Li+^{115}In reactions. The experiment for the ^{7}Li+^{115}In system was performed at the BARC-TIFR Pelletron facility in Mumbai, India. The off-beam γ-spectroscopy technique was adopted, and the radionuclides used in the current analysis were identified following their characteristic γ-rays and the decay curve. The measured cross sections of ^{92m}Nb and ^{116m}In were significantly underpredicted by the calculations performed using the PACE4 and EMPIRE nuclear reaction codes, which are based on equilibrium and

pre-equilibrium reaction processes. Consequently, we examined their production via the one-neutron transfer channel. The CRC calculations were carried out using the FRESCO code framework [38].

The coupling scheme adopted for neutron transfer in the ^{6}Li+^{93}Nb reaction is shown in Fig. 1. The calculations employed the double-folding SPP [11, 12] for both the real and imaginary parts of the OP ($U(R) = (N_r + iN_i)V^{SP}(R)$). In the entrance partition, the strength coefficients for the real and imaginary potentials were set to $N_r = N_i = 0.6$, following previous studies [28, 29, 39–41], to account for flux loss due to dissipative and breakup channels [40, 41] and the repulsive nature of the real part of the breakup polarization potential [42–45]. In the exit partition, the SPP was used for the real and imaginary components with strength coefficients $N_r = 1.0$ and $N_i = 0.78$ [46], respectively. A coefficient value of 0.78 has been proven effective for describing the elastic scattering cross section for various systems, spanning wide ranges of masses and energies [47]. The prior form of potential with full complex remnant terms and non-orthogonality corrections were included in the calculations. The Woods-Saxon form factor with a radius of $1.27A^{1/3}$ fm and a diffuseness of 0.65 fm for both lighter and heavier nuclei, where A represents the mass of the core nucleus, was utilized to generate single-particle wave functions. The depth was adjusted to reproduce the binding energy of the particle-core composite system, and a spin-orbit component was also included.

In the ^{7}Li+^{115}In reaction, the spectroscopic amplitudes for target overlaps were set equal to 1.0, as accurately determining these amplitudes requires a large model space, which is challenging to handle computationally. The coupling scheme depicted in Fig. 2 was employed in the calculations. Table 3 provides the spectroscopic data related to the target overlaps. For these calculations, the

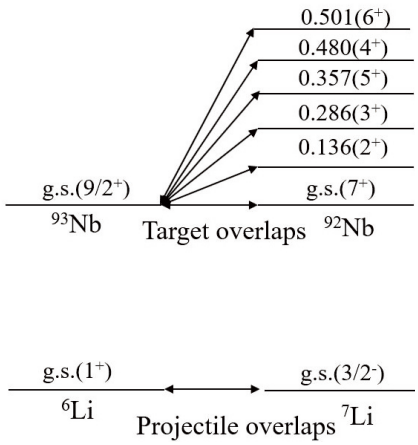

Fig. 1. Coupling scheme considered in the one-neutron transfer calculation for the ^{6}Li+^{93}Nb reaction. The energies of the states are in megaelectronvolts.

SPP was used for both the real and imaginary parts of the OP. The strength coefficients for the real and imaginary potentials were set to $N_r = N_i = 0.6$ in the entrance partition. In the final partition, the SPP was utilized for the real and imaginary parts with strength coefficients of $N_r = 1.0$ and $N_i = 0.78$, respectively. The calculations were performed using the post form of the potential, including

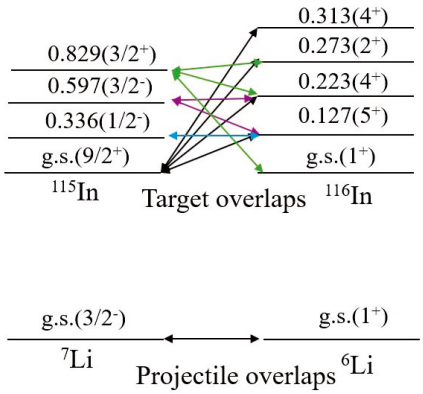

Fig. 2. Coupling scheme considered in one-neutron transfer calculations for the ^{7}Li+^{115}In reaction. The energies of the states are in megaelectronvolts.

Table 3. Spectroscopic amplitudes used in one-neutron transfer CRC calculations for the ^{7}Li+^{115}In reaction, where j is the spin of the neutron orbitals.

Initial State	j	Final State	Spect. Ampl.
$^{115}\mathrm{In}_{g.s.}(9/2^+)$	$3s_{1/2}$	$^{116}\mathrm{In}_{0.127}(5^+)$	1.0
	$2d_{3/2}$		1.0
	$2d_{5/2}$		1.0
$^{115}\mathrm{In}_{g.s.}(9/2^+)$	$3s_{1/2}$	$^{116}\mathrm{In}_{0.223}(4^+)$	1.0
	$2d_{3/2}$		1.0
	$2d_{5/2}$		1.0
$^{115}\mathrm{In}_{g.s.}(9/2^+)$	$2d_{5/2}$	$^{116}\mathrm{In}_{0.273}(2^+)$	1.0
$^{115}\mathrm{In}_{g.s.}(9/2^+)$	$3s_{1/2}$	$^{116}\mathrm{In}_{0.313}(4^+)$	1.0
	$2d_{3/2}$		1.0
	$2d_{5/2}$		1.0
$^{115}\mathrm{In}_{0.336}(1/2^-)$	$1h_{11/2}$	$^{116}\mathrm{In}_{0.127}(5^+)$	1.0
$^{115}\mathrm{In}_{0.597}(3/2^-)$	$1h_{11/2}$	$^{116}\mathrm{In}_{0.127}(5^+)$	1.0
$^{115}\mathrm{In}_{0.597}(3/2^-)$	$1h_{11/2}$	$^{116}\mathrm{In}_{0.223}(4^+)$	1.0
$^{115}\mathrm{In}_{0.829}(3/2^+)$	$3s_{1/2}$	$^{116}\mathrm{In}_{g.s.}(1^+)$	1.0
	$2d_{3/2}$		1.0
	$2d_{5/2}$		1.0
$^{115}\mathrm{In}_{0.829}(3/2^+)$	$2d_{5/2}$	$^{116}\mathrm{In}_{0.223}(4^+)$	1.0
$^{115}\mathrm{In}_{0.829}(3/2^+)$	$3s_{1/2}$	$^{116}\mathrm{In}_{0.273}(2^+)$	1.0
	$2d_{3/2}$		1.0
	$2d_{5/2}$		1.0

full complex remnant term and non-orthogonality corrections. The potentials binding the transferred particles were of the Woods-Saxon type, with a radius of $1.27A^{1/3}$ fm for (both) lighter and heavier nuclei and a diffuseness of 0.65 fm. The spin-orbit interaction was also included.

2. *Two-neutron transfer*

In order to study the production of ^{183}Ta through the two-neutron transfer channel in the ^{7}Li+^{181}Ta reaction [23], we examined the simultaneous transfer of two neutrons using the extreme cluster approach, where the spectroscopic amplitudes for target and projectile overlap were taken as unity. This approach considers the transition potential to act on the relative motion between the correlated nucleon pair and the core. This approach treats the pair of nucleons as a single quasi-particle. The wave function of the cluster is derived from the energy conservation relation of the harmonic oscillator [1]:

$$\sum_{i=1}^{2} 2(n_i-1)+l_i = 2(N-1)+L+2(n-1)+l. \qquad (4)$$

Here, n_i and l_i represent the principal quantum number and orbital angular momentum of individual nucleons. The symbols n,l and N,L denote the corresponding quantities for the motion of the nucleons relative to each other and to the core. In the extreme cluster approximation, the two-nucleon cluster is assumed to be in the $1s$ internal state $(n=1,l=0)$ with an intrinsic spin $S=0$ (anti-parallel spin configuration).

In Ref. [23], ^{183}Ta produced in the ^{7}Li+^{181}Ta reaction was identified using offline γ-spectroscopy, and the measured cross section of ^{183}Ta was compared with those calculated using EMPIRE with GC, GSM, and EGSM level densities. The calculations underestimated the experimental data by 4 to 5 orders of magnitude. Consequently, we examined the production of ^{183}Ta through the two-neutron transfer channel. The coupling scheme shown in Fig. 3 was used in the calculations. The initial and final bound state wave functions for the di-neutron system were generated using a Woods-Saxon potential, with a radius of 1.30 fm and diffuseness of 0.70 fm. The depth of the potential was adjusted to match the two-neutron separation energy. The finite range transfer calculations were performed using the post form of the interaction potential, incorporating the full complex remnant term and non-orthogonality corrections. The SPP was employed as the OP for both the real and imaginary components. A strength coefficient of 0.6 was applied to the real and imaginary parts in the entrance partition. In the final partition, the imaginary part was scaled by a factor of 0.78. We also used the spin-orbit interaction term.

However, the nucleus ^{5}Li is unstable and decays into

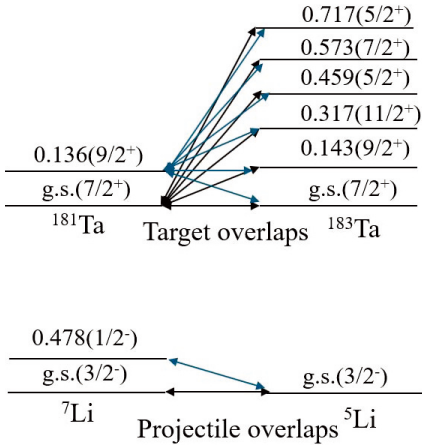

Fig. 3. Coupling scheme considered in the two-neutron transfer calculation for the ^{7}Li+^{181}Ta reaction. The energies of the states are in megaelectronvolts.

^{4}He and a proton. For the overlap $\langle^{7}\text{Li}|^{5}\text{Li}\rangle$, we considered the first step in the CRC calculations, where the ground-state resonance of ^{5}Li is formed and subsequently decays. If this resonance exists for a sufficient duration, it can be treated as a bound state in CC calculations. It is a standard method in CC calculations for explaining broad resonances, such as those in ^{6}Li and ^{7}Li [48].

D. Discussion

We performed the CRC calculations using the code FRESCO to confirm that the residues ^{92m}Nb, ^{116m}In, and ^{183}Ta result from transfer reactions. These calculations examined the production of ^{92m}Nb via one-neutron pickup in ^{6}Li-induced reaction on ^{93}Nb, ^{116m}In via one-neutron stripping in ^{7}Li-induced reaction on ^{115}In, and ^{183}Ta via two-neutron stripping in ^{7}Li-induced reaction on ^{181}Ta. The results of these calculations are presented in Figs. 4, 5, and 6 and are compared with the experimental data. The solid black lines represent the CRC calculation results, incorporating the SPP with parameters N_r=N_i = 0.60 for the entrance channel and N_r=1.0, N_i=0.78 for the exit channel in all three reactions. The figures indicate that the calculations closely match the experimental data in all cases. The CRC calculations using the extreme cluster model describe the data well for transferring two neutrons in the ^{7}Li-induced reaction on ^{181}Ta, indicating the dominance of the one-step reaction mechanism.

Although the SPP was utilized as the OP, the single-particle states were generated using Woods-Saxon form factors for projectile and target overlaps. These form factors have three parameters: depth, reduced radius, and diffuseness. The sensitivity of the transfer cross section to changes in the reduced radius was analyzed and is presented in Figs. 7, 8, and 9. The excitation functions for transfer in all three reactions were studied at three reduced radii values: 1.20 fm, 1.25 fm, and 1.3 fm, commonly re-

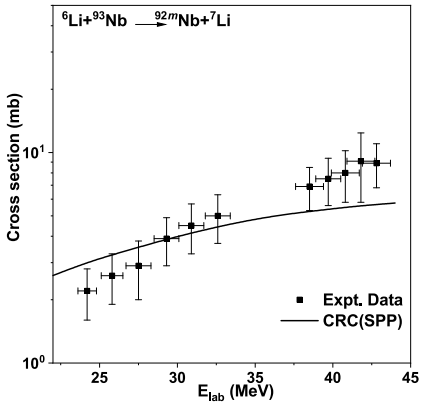

Fig. 4. Comparison between experimental results [21] and the theoretical excitation function for the reaction ^{93}Nb(^{6}Li,^{7}Li)^{92m}Nb.

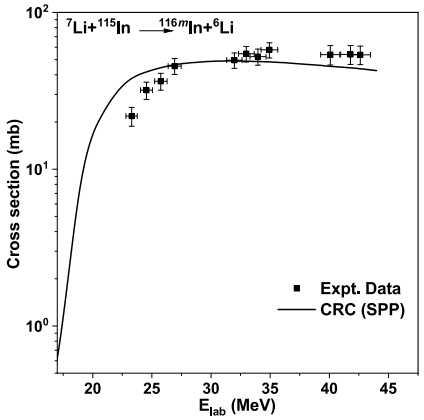

Fig. 5. Comparison between experimental results and the theoretical excitation function for the reaction ^{115}In(^{7}Li,^{6}Li)^{116m}In.

ported in the literature. Increasing or decreasing these parameters for both the projectile and target form factors clearly leads to a corresponding increase or decrease in the transfer cross section compared to the average value of this parameter. Based on this analysis, the value of r used was 1.27 fm for one-neutron transfer reactions and 1.30 fm for two-neutron transfer reactions.

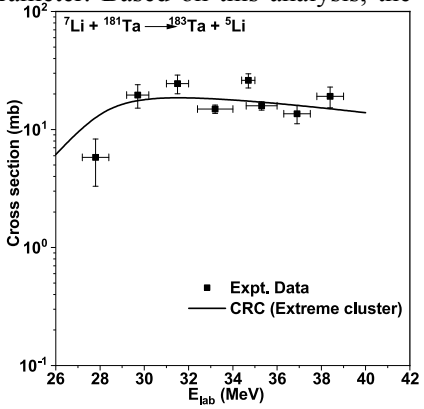

Fig. 6. Comparison between experimental results [23] and the theoretical excitation function for the reaction ^{181}Ta(^{7}Li,^{5}Li)^{183}Ta.

Individual transitions were not measured because the nuclei of interest were measured using γ-spectroscopy. Understanding the individual transitions and the population pattern of transfer products, as derived from experiments, will offer deeper insights into the underlying reaction mechanism.

III. SUMMARY

We conducted CRC calculations to understand the mechanism of one-neutron transfer in the ^{93}Nb(^{6}Li, ^{7}Li)^{92m}Nb and ^{115}In(^{7}Li,^{6}Li)^{116m}In reactions and two-neutron transfer in the ^{181}Ta(^{7}Li,^{5}Li)^{183}Ta reaction. The double folding SPP was utilized, with the adopted imaginary potential $W(R) = N_i \times V_{\rm SPP}$. We thoroughly examined the one-neutron transfer in the ^{6}Li+^{93}Nb and ^{7}Li+^{115}In reactions, as well as the two-neutron transfer in the ^{7}Li+^{181}Ta reaction, including the low lying excited

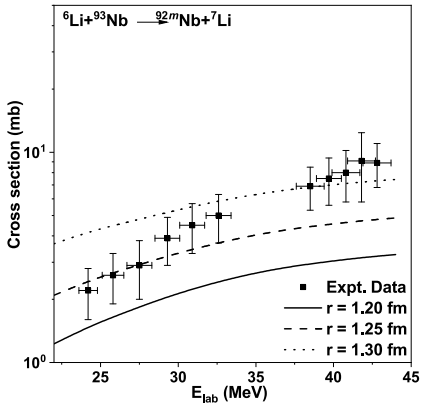

Fig. 7. Effects of variations in the reduced radius of the form factor of the projectile and target overlaps on the one-neutron transfer cross section for the ^{93}Nb(^{6}Li,^{7}Li)^{92m}Nb reaction. The experimental data were taken from Ref. [21].

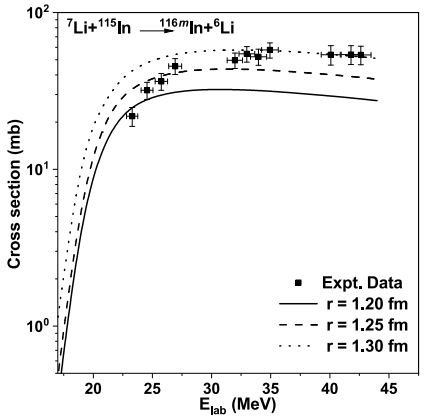

Fig. 8. Effects of variations in the reduced radius of the form factor of the projectile and target overlaps on the one-neutron transfer cross section for the ^{115}In(^{7}Li,^{6}Li)^{116m}In reaction.

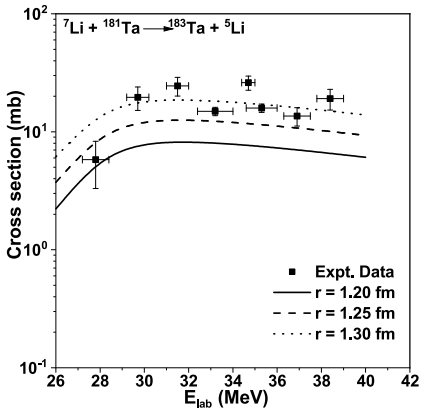

Fig. 9. Effects of variations in the reduced radius of the form factor of the projectile and target overlaps on the two-neutron transfer cross section for the ^{181}Ta(^{7}Li,^{5}Li)^{183}Ta reaction. The experimental data were taken from Ref. [23].

states of both the projectile and the target. The simultaneous transfer of two neutrons in the ^{7}Li+^{181}Ta reaction was studied using the extreme cluster model. The optimal values of N_i for the initial and final partitions were found to be 0.6 and 0.78 for all three systems. A reasonable agreement between the experimental and theoretical cross sections was achieved in this study. The effects of the reduced radius of the form factor of the projectile and the target on the transfer cross sections were also studied. More systematic investigations of multinucleon transfer channels within the CRC framework would help constrain potential parameters and reduce uncertainties in state selection. Identifying γ-transitions in coincidence with reaction products would allow for a more precise choice of states to include in the calculations, leading to a deeper understanding of the transfer mechanisms.

ACKNOWLEDGMENTS

The authors sincerely thank their colleagues from the TASISPEC Lab for their support, Mr. Chandra Kumar for the valuable discussions, and Dr. Erica N. Cardozo regarding the FRESCO calculations.

References

[1] G. R. Satchler, *Direct Nuclear Reactions* (Oxford: Oxford University Press, 1983).
[2] C. H. Dasso, G. Pollarolo, and A. Winther, Phys. Rev. Lett. **73**, 1907 (1994)
[3] R. Broda, J. Phys. G: Nucl. Part. Phys. **32**, R151 (2006)
[4] N. Keeley, R. Raabe, N. Alamanos *et al.*, Prog. Part. Nucl. Phys. **59**, 579 (2007)
[5] N. Keeley, N. Alamanos, K. W. Kemper *et al.*, Prog. Part. Nucl. Phys. **63**, 396 (2009)
[6] W. von Oertzen and A. Vitturi, Rep. Prog. Phys. **64**, 1247 (2001)
[7] C. Agodi, G. Giuliani, F. Cappuzzello *et al.*, Phys. Rev. C **97**, 034616 (2018)
[8] M. C. Mermaz, C. A. Whitten, J. W. Champlin *et al.*, Phys. Rev. C **4**, 1778 (1971)
[9] R. Peterson, C. Fields, R. Raymond *et al.*, Nucl. Phys. A **408**, 221 (1983)
[10] K. Pearce, N. Clarke, R. Griffiths *et al.*, Nucl. Phys. A **467**, 215 (1987)
[11] L. C. Chamon, D. Pereira, M. S. Hussein *et al.*, Phys. Rev. Lett. **79**, 5218 (1997)
[12] L. C. Chamon, B. V. Carlson, L. R. Gasques *et al.*, Phys. Rev. C **66**, 014610 (2002)
[13] A. Shrivastava, A. Navin, A. Lemasson *et al.*, Phys. Rev. Lett. **103**, 232702 (2009)
[14] A. Shrivastava, A. Navin, A. Diaz-Torres *et al.*, Phys. Lett. B **718**, 931 (2013)
[15] C. S. Palshetkar, S. Thakur, V. Nanal *et al.*, Phys. Rev. C **89**, 024607 (2014)
[16] R. Kumar, R. Prajapat, and M. Maiti, J. Phys. G: Nucl. Part. Phys. **50**, 025106 (2023)
[17] A. Chatterjee, A. Navin, A. Shrivastava *et al.*, Phys. Rev. Lett. **101**, 032701 (2008)
[18] A. Lemasson, A. Shrivastava, A. Navin *et al.*, Phys. Rev. Lett. **103**, 232701 (2009)
[19] R. Raabe, J. L. Sida, J. L. Charvet *et al.*, Nature (London) **431**, 823 (2004)
[20] R. Prajapat and M. Maiti, Phys. Rev. C **103**, 034620 (2021)
[21] A. Singh and M. Maiti, Phys. Rev. C **107**, 054610 (2023)
[22] R. Prajapat and M. Maiti, Phys. Rev. C **101**, 024608 (2020)
[23] A. Chauhan and M. Maiti, Phys. Rev. C **99**, 034608 (2019)
[24] S. P. Hu, G. L. Zhang, J. C. Yang *et al.*, Phys. Rev. C **91**, 044619 (2015)
[25] V. Jha, V. V. Parkar, and S. Kailas, Phys. Rep. **845**, 1 (2020)
[26] M. K. Pradhan, A. Mukherjee, S. Roy *et al.*, Phys. Rev. C **88**, 064603 (2013)
[27] A. Shrivastava, A. Navin, N. Keeley *et al.*, Phys. Lett B **633**, 463 (2006)
[28] S. P. Hu, G. L. Zhang, J. C. Yang *et al.*, Phys. Rev. C **93**, 014621 (2016)
[29] Y. D. Fang, P. R. S. Gomes, J. Lubian *et al.*, Phys. Rev. C **93**, 034615 (2016)
[30] V. V. Parkar, S. K. Sharma, R. Palit *et al.*, Phys. Rev. C **97**, 014607 (2018)
[31] S. K. Pandit, A. Shrivastava, K. Mahata *et al.*, Phys. Rev. C **96**, 044616 (2017)
[32] G. L. Zhang, G. X. Zhang, S. P. Hu *et al.*, Phys. Rev. C **97**, 014611 (2018)
[33] G. R. Satchler and W. G. Love, Phys. Rep. **55**, 183 (1979)
[34] M. El-Azab Farid and G. R. Satchler, Nucl. Phys. A **438**, 525 (1985)
[35] L. C. Chamon, B. Carlson, and L. Gasques, Comput. Phys. Commun. **267**, 108061 (2021)
[36] B. A. Brown and W. D. M. Rae, Nucl. Data Sheets **120**, 115 (2014)
[37] S. Cohen and D. Kurath, Nucl. Phys. A **101**, 1 (1967)
[38] I. J. Thompson, Comput. Phys. Rep. **7**, 167 (1988)
[39] V. V. Parkar, A. Parmar, Prasanna M *et al.*, Phys. Rev. C **104**, 054603 (2021)

[40] D. P. Sousa, D. Pereira, J. Lubian *et al*., Nucl. Phys. A **836**, 1 (2010)
[41] D. Pereira, J. Lubian, J. R. B. Oliveira *et al*., Phys. Lett. B **670**, 330 (2009)
[42] R. S. Mackintosh and N. Keeley, Phys. Rev. C **79**, 014611 (2009)
[43] V. V. Parkar, I. Martel, A. M. Sánchez-Benítez *et al*., Acta Phys. Pol. **42**, 761 (2011)
[44] V. V. Parkar, V. Jha, S. K. Pandit *et al*., Phys. Rev. C **87**, 034602 (2013)
[45] S. Santra, S. Kailas, K. Ramachandran *et al*., Phys. Rev. C **83**, 034616 (2011)
[46] L. R. Gasques, M. Dasgupta, D. J. Hinde *et al*., Phys. Rev. C **74**, 064615 (2006)
[47] L. R. Gasques, L. C. Chamon, P. R. S. Gomes *et al*., Nucl. Phys. A **764**, 135 (2006)
[48] M. Dasgupta, P. R. S. Gomes, D. J. Hinde *et al*., Phys. Rev. C **70**, 024606 (2004)